JSINE : Vol. 1, Issue 1, 2021, Page 08–16 ISSN (Online) 2583-2093

Journal of Science Innovations and Nature of Earth

Journal homepage : www.jsiane.com

HERSCHEL-BULKLEY FLUID: STUDY OF RHEOLOGICAL PROPERTIES FOR BLOOD FLOW OF PULSES IN ω-PROTOTYPE IN ARTERIES' STENOSIS

Pawan Kumar
IET, Dr. Shakuntala Misra National Rehabilitation University, Lucknow- 226017
satgurukripadrpawan@gmail.com

Abstract

In this article, we examined the blood flow that was being pressed as part of the war. The Herschel-Bulkley fluid model is applied for representing non-Newtonian blood features in the small arteries. The current governing equation is guided by the fact that the flow has shape and is linear. The standard method of cleanup is used to get first-order expressions for different flow variables. The temporal distributions of axial velocity and wall shear stress, flow meter flow rate and flow resistance are shown in bold. Also discussed are the parameters involved in the contact of various fields of impact plug-flow. A comparison of blood flow and stimulus signals in the same area also causes the blood vessels to recover. All content is an article licensed underneath of a Creative Commons Attribution (CC BY) licence, if not in writing.

Keywords : Non-Newtoian fluid, Herschel-Bulkley fluid model, Rheological Properties

Received 20.01.2021 **Revised 15.02.2021** **Accepted 20.02.2021**

Introduction

Various medical studies show that the cardiovascular system activates more than 80 per cent of deaths in human organisms. Heart disease is closely linked to the geometry of blood flow and the blood vessels. Stenosis causes the arteries to get blood flow. Stenosis helps to lower blood pressure.

Under conditions of disease the vein becomes larger and may lead to stenosis formation. Dwivedi was involved along with others.[1] The fluid flow in a small duct tube was examined and it indicated that the blood vessels were connected and pressed into the space flow. One of the main causes of hypertension is the tapping position of hypertension and according to Chathuri and Prahlada[2], the greater variation in pressure is apparent at smaller angles (up to 2). Therefore it's important to research blood flow in most dilated veins. Viscosity, non-Newtonian blood flow, and the geometric names of blood vessels play an important role in blood transportation in the circulatory system. The blood plasma displays a suspension of cells, indicating incompatibility. Newtonian blood properties are expressed in large veins with a high rate of shear, while blood in small veins has a non-Newtonian character with a high rate of shear.[3] The literature depicts the main stenotic components on the Newtonian blood flow.4-10 Several researchers have also used a particular non-Newtonian model to investigate arterial blood flow via mild stenosis. Symptoms of the blood flow are severely impacted by stenosis. Nadeem et al[11] had analyzed effects of stenotic vessels on the power flow of the power law. The square and equilateral [12] purification method was used to test the arterial blood flow using the Kaizen Fluid model. Shukla *et al.*[13] Mirza *et al*. The effect of soluble cells on non-Newtonian blood flow was investigated, which treats the effects of shear stress and excitation disorders as non-Newtonian fluids. A blood flow study using the methods of CrossRule, Carrieu, Herschel-Bulkley, Oldroid-B alcohol and Cisco to terpenes stenotic veins[14-21] Ratan Shah[22] performs the Sapna. Congenital behavior on Non-Symmetric Multiple Steno Artery in the Newtonian Radial. Nikolaev et al.[23] Measuring intracranial aneurysm blood flow problem. Shankar[24] predicts blood flow through arterial stenosis which is non-symmetric. Siddiqui *et al.*[25] had observed pulsatile flow of kaizen fluid. All of these studies did blood flow to the artery's stenotic region. Stenosis, however, can develop in a number of ways, and can take the form of a bookcase. We 're inspired by the fact Chakravarti *et al*[26] observed the impact[27] of stenosis on blood flow. By Since Herschel-The steady flow of bulky fluid saturated the decisive part of the battle that Prasad *et al.*[28] were analyzing. The flow of small microprocessor fluid through tapped coated veins was discussed by Srikanth *et al.*[29]. Hybridity and Hematology30 is said to be the most common method of fluctuation, so that one can study Herschel 's horizontal flow-Bulkley fluid in a single sound.

Inspired by the above discussion, an attempt was made to look through a dissected artery at the Herschel-Bulkley fluid with complete stenosis. In computers with cylindrical polar area, the current flow of control data is determined. Shankar's method is used to find the exchange mechanism solution, shear wall strain, resistance impedance, and plug core length, as well as the hemalata 30. The effect of different parameters on the characterization of the flow of transformed, chaotic and unsaturated arteries is examined in depth. The results from the present study equate Shankar and Hemalatha 's findings.[30]

Problem Definition

You expect blood to flow through the artery of the tube. The problem is based on organic cylindrical compounds. Let R and the axes be taken, respectively, from the radiation axis and the artery. It's in the ways of these cycles. Figure 1 shows

the geometric structure of the ered-stamped cemented stenomed wall and Mathematically defined.[29]

$$\overline{R}(\overline{z}) = \begin{cases} (\overline{\xi}\overline{z} + \overline{R}_0) + \frac{3}{2}\frac{\overline{\epsilon}}{\overline{L}_0^3}\left[36(\overline{z}-\overline{d})^4 - 72(\overline{z}-\overline{d})^3\overline{L}_0 + 47(\overline{z}-\overline{d})^2\overline{L}_0^2 - 11(\overline{z}-\overline{d})\overline{L}_0^3\right], & \overline{d} \le \overline{z} \le \overline{L}_0 + \overline{d} \\ (\overline{\xi}\overline{z} + \overline{R}_0) & \text{otherwise} \end{cases} \quad (1)$$

R_0 is the fixed radius of the normal artery of nonstenotic area, d = the stenotic area, the stenosis length is st, the stenosis height is the critical height, R (z) = the artery through which the damaged radiation occurs, and the artery slope ξ= (tan ψ) is taped.

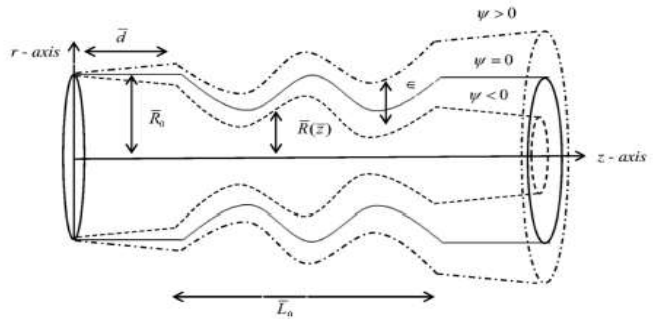

FIG. 1. Geometry of overlapping stenosed artery.

With angle of ψ. ψ> 0, ψ<0 and ψ = 0 respectively do not scan, change and click the artery. In the form of an invisible, fully developed, and Herschel-a bulky zen-flowing arterial shape that runs through the stenotic shaped area. Radial velocity is undesirable when stenosis occurs for low Reynolds number. In these cases this is an important statistical

$$\frac{\partial \overline{w}}{\partial \overline{t}} = -\frac{1}{\overline{\rho}}\frac{\partial \overline{p}}{\partial \overline{z}} - \frac{1}{\overline{r}}\frac{1}{\overline{\rho}}\frac{\partial}{\partial \overline{r}}(\overline{r}\,\overline{\tau}), \quad (2)$$

$$\frac{\partial \overline{p}}{\partial \overline{r}} = 0, \quad (3)$$

Where w = velocity in axial direction is shear stress, p =pressure & ÿ = −πrz. Herschel's constitutive equation-Bulkley fluid is

$$\overline{\tau}_{rz} = \overline{\mu}_H^{1/m}\left(-\frac{\partial \overline{w}}{\partial \overline{r}}\right)^{1/m} + \overline{\tau}_y \text{ if } \overline{\tau}_{rz} \ge \overline{\tau}_y, \quad (4)$$

$$\frac{\partial \overline{w}}{\partial \overline{r}} = 0 \text{ if } \overline{\tau}_{rz} < \overline{\tau}_y, \quad (5)$$

where $\overline{\tau}_y$ y = yield stress & $\overline{\mu}_H$ = coefficient of viscosity for Herschel-Bulkley fluid.

Stress & velocity boundary conditions on the arterial wall

$$\overline{\tau}\Big|_{\overline{r}=0} \text{ is finite} \quad (6)$$

$$\overline{w}\Big|_{\overline{r}=\overline{R}(\overline{z})} = 0 \quad (7)$$

It is assumed that the pressure gradient depends on z & t. That is mathematically expressed as

$$\frac{\partial \overline{p}}{\partial \overline{z}} = -d(\overline{t})\overline{q}(\overline{z}), \quad (8)$$

Where q q(z . A parameters are flow amplitude & Blood angular frequency respectively; To normalize regulating equations & boundary conditions, we define

$$t = \overline{t}\,\overline{\omega}, \; r = \frac{\overline{r}}{\overline{R}_0}, \; z = \frac{\overline{z}}{\overline{L}_0}, \; q(z) = \frac{\overline{q}(\overline{z})}{\overline{q}_0}, \; \theta = \frac{2\,\overline{\tau}_y}{\overline{q}_0\overline{R}_0}, \; w = \frac{\overline{w}}{\overline{q}_0\,\overline{R}_0^2/4\overline{\mu}_0}, \; \alpha^2 = \frac{\overline{R}_0^2\overline{\omega}\,\overline{\rho}}{\overline{\mu}_0}, \; \tau = \frac{\overline{\tau}}{\overline{q}_0\,\overline{R}_0/2},$$

$$\epsilon = \frac{\overline{\epsilon}}{\overline{R}_0}, \; d = \frac{\overline{d}}{\overline{R}_0}, \; R(z) = \frac{\overline{R}(\overline{z})}{\overline{R}_0}, \; \xi = \frac{\overline{\xi}\,\overline{L}_0}{\overline{R}_0}, \; L_0 = \frac{\overline{L}_0}{\overline{R}_0}. \quad (9)$$

Where μ μ = μ μH[2/q_0R_0]m^{-1}, q_0 = pressure gradient negative in normal artery & α= Wormersly frequency parameter. By using variables without dimensions Eqs. Converts (2)–(5)

$$\alpha^2\frac{\partial w}{\partial t} = -2\left\{2d(t)q(z) + \frac{1}{r}\frac{\partial(r\,\tau)}{\partial r}\right\} \quad (10)$$

$$\tau_{rz} = \theta + \left(-\frac{1}{2}\frac{\partial w}{\partial r}\right)^{1/m}, \text{ if } \tau_{rz} \ge \theta \quad (11)$$

$$\frac{\partial w}{\partial r} = 0, \text{ if } \tau_{rz} < \theta \quad (12)$$

In which d(t) = 1 + Asin t. Non-dimensional limit conditions are

$$\tau\Big|_{r=0} \text{ is finite} \quad (13)$$

$$w\Big|_{r=R(z)} = 0 \quad (14)$$

Arterial wall geometry in dimensionless form

$$R(z) = \begin{cases} (\xi z + 1) + \frac{3\epsilon}{2}\left[36(z-\beta)^4 - 72(z-\beta)^3 + 47(z-\beta)^2 - 11(z-\beta)\right], & \beta \le z \le 1+\beta \\ (\xi z + 1) & \text{otherwise} \end{cases} \quad (15)$$

where $\beta = \frac{d}{L_0}$.

Method of Solution

It is worthy of note that Q 2 occurs naturally in the Eq. (10) and relates to the volatile term. Rising the dependent variable according to variable 2 is therefore necessary. Take the following attribute Dependence:

$$w(t,r,z) = w_0(t,r,z) + \alpha^2 w_1(t,r,z) + \ldots, \quad (16)$$

$$\tau(t,r,z) = \tau_0(t,r,z) + \alpha^2\tau_1(t,r,z) + \ldots, \quad (17)$$

$$R_p(t,z) = R_{0p}(t,z) + \alpha^2 R_{1p}(t,z) + \ldots, \quad (18)$$

$$w_p(t,z) = w_{0p}(t,z) + \alpha^2 w_{1p}(t,z) + \ldots, \quad (19)$$

$$\tau_p(t,z) = \tau_{0p}(t,z) + \alpha^2\tau_{1p}(t,z) + \ldots, \quad (20)$$

From the above equations, the frequency effects for the small values of the frequency parameters are found to be not important. Replacing the words (16) and (17) into Eq. (10) and the equality of term α 2 coefficients, we have

$$\frac{\partial(r\,\tau_0)}{\partial r} = 2rd(t)q(z) \tag{21}$$

$$\frac{\partial w_0}{\partial t} = -\frac{2}{r}\frac{\partial}{\partial r}(\tau_1 r) \tag{22}$$

Including Eq. (21) In the case of r from 0 to R0p & the condition that ÿp is finite at r = 0, we get

$$\tau_{0p} = d(t)q(z)R_{0p} \tag{23}$$

Now to get Ś0, Eq. (21) shall be integrated in favor of r

$$\tau_0 = q(z)d(t)r \tag{24}$$

where Eq. (23) is used to eliminate R^{0p}. Substituting expression (16) & (17) into Eq. (11), one finds

$$\frac{\partial w_0}{\partial r} = -2(\tau_0 - m\theta)\,\tau_0^{m-1} \tag{25}$$

$$\frac{\partial w_1}{\partial r} = -2m(\tau_0 - (m-1)\theta)\tau_0^{m-2}\tau_1 \tag{26}$$

Inserting values of τ_0 in Eq. (24) into Eq. (25), integrating w.r.t. r in interval [r, R] & then utilizing boundary condition (14)

where $\kappa^2 = \theta/d(t)q(z)$. Plug core velocity is computed from Eq. (27) as

$$w_0 = 2(d(t)q(z))^m R\left[\frac{1}{(m+1)}\left\{1-\left(\frac{r}{R}\right)^{m+1}\right\} - \frac{\kappa^2}{R}\left\{1-\left(\frac{r}{R}\right)^{m}\right\}\right], \tag{27}$$

$$w_{0p} = 2(d(t)q(z))^m R\left[\frac{1}{(m+1)}\left\{1-\left(\frac{R_{0p}}{R}\right)^{m+1}\right\} - \frac{\kappa^2}{R}\left\{1-\left(\frac{R_{0p}}{R}\right)^{m}\right\}\right] \tag{28}$$

Eq. (23) expression of R^{0p} is

$$R_{0p} = \frac{\theta}{d(t)q(z)} = \kappa^2, \tag{29}$$

Where π0p = equivalent is used. Solve Eqs. (22) & (26), using Eqs. (27) & (28) & use cap conditions (13) & (14)

$$\tau_{1p} = -(d(t)q(z)R)^m R^2 D\left[\frac{m}{2(m+1)}\left(\frac{\kappa^2}{R}\right) - \frac{m}{2}\left(\frac{\kappa^2}{R}\right)^2 + \frac{m^2}{2(m+1)}\left(\frac{\kappa^2}{R}\right)^{m+2}\right] \tag{30}$$

$$\tau_1 = -m(d(t)q(z)R)^m R^2 D\left[\frac{1}{(m+1)(m+3)}\left\{\left(\frac{m+3}{2}\right)\left(\frac{r}{R}\right) - \left(\frac{r}{R}\right)^{m+2}\right\}\right.$$
$$\left. -\left(\frac{\kappa^2}{R}\right)\left(\frac{1}{m+2}\right)\left\{\left(\frac{m+2}{2}\right)\left(\frac{r}{R}\right) - \left(\frac{r}{R}\right)^{m+1}\right\} + \frac{m^2+2m-2}{(m+3)(2m+4)}\left(\frac{R}{r}\right)^{m+2}\left(\frac{\kappa^2}{R}\right)^{m+3}\right] \tag{31}$$

$$w_1 = -2m^2(d(t)q(z)R)^{2m-1}DR^3\left[\frac{1}{(m+1)^2(2m+6)}\left\{(m+3)\left(\frac{r}{R}\right)^{m+1} - \left(\frac{r}{R}\right)^{2m+2} - (m+2)\right\}\right.$$
$$-\frac{\kappa^2}{R}\left\{\frac{1}{2m+2}\left(\left(\frac{r}{R}\right)^{m+1}+1\right) + \frac{m-1}{(m+1)(m+3)}\left\{\frac{m+3}{2m}\left(\frac{r}{R}\right)^m - \frac{1}{2m+1}\left(\frac{r}{R}\right)^{2m+1}\right.\right.$$
$$\left.\left. + \frac{m+3}{2m} - \frac{1}{2m+1}\right\}\right\} - \frac{m-1}{2m}\left(\frac{\kappa^2}{R}\right)^2\left(\left(\frac{r}{R}\right)^m - \left(\frac{r}{R}\right)^{2m}\right) + \frac{m^2+2m-2}{(m+2)(m+3)(m-1)}\left(\frac{r}{R}\right)^{m+3}$$
$$\left.\times\left(\left(\frac{r}{R}\right)^{m-1} - 1\right) - \frac{m^2+2m-2}{(m+3)(m-2)(2m+4)}\left(1-\left(\frac{r}{R}\right)^{m-2}\right)\left(\frac{r}{R}\right)^{m+4}\right] \tag{32}$$

$$w_{1p} = -2m^2(d(t)q(z)R)^{2m-1}DR^3\left[\frac{1}{(m+1)^2(2m+6)}\left\{(m+3)\left(\frac{\kappa^2}{R}\right)^{m+1} - \left(\frac{\kappa^2}{R}\right)^{2m+2} - (m+2)\right\}\right.$$
$$-\frac{\kappa^2}{R}\left\{\frac{1}{2m+4}\left(\left(\frac{\kappa^2}{R}\right)^{m+1}+1\right) + \frac{m-1}{(m+1)(m+3)}\left\{\frac{m+3}{2m}\left(\frac{\kappa^2}{R}\right)^m - \frac{1}{2m+1}\left(\frac{\kappa^2}{R}\right)^{2m+1}\right.\right.$$
$$\left.\left. + \frac{m+3}{2m} - \frac{1}{2m+1}\right\}\right\} - \frac{m-1}{2m}\left(\frac{\kappa^2}{R}\right)^2\left(\left(\frac{\kappa^2}{R}\right)^m - \left(\frac{\kappa^2}{R}\right)^{2m}\right) + \frac{m^2+2m-2}{(m-1)(m+2)(m+3)}\left(\frac{\kappa^2}{R}\right)^{m+3}$$
$$\left.\times\left(\left(\frac{\kappa^2}{R}\right)^{m-1} - 1\right) + \frac{m^2+2m-2}{(2m+4)(m+3)(m-2)}\left(\frac{\kappa^2}{R}\right)^{m+4}\left(\left(\frac{\kappa^2}{R}\right)^{m-2} - 1\right)\right], \tag{33}$$

where D =(1/d(t))*((d(d(t))/dt). final expression of axial velocity w can be obtained from Eq. (16), (27) & (32). Wall shear stress is

$$\tau_w = (d(t)q(z)R)\left[1 - \frac{(\alpha^2 R^2 D)(q(z)d(t)R)^{m-1}}{(2m+4)(m+3)}\left\{(m+2) - m(m+3)\left(\frac{\kappa^2}{R}\right) + (m^2+2m-2)\left(\frac{\kappa^2}{R}\right)^{m+3}\right\}\right]. \quad (34)$$

From formula Q(z, t) = 4 $\int_0^R w(r,z,t)rdr$, volumetric flow rate turns out to be

$$Q(t,z) = -2m^2(d(t)q(z))^{2m-1}DR^5\left[\frac{1}{(m+1)^2(2m+6)}\left\{-\frac{2m^2+m+2}{4m+2} + \frac{m+1}{2}\left(\frac{\kappa^2}{R}\right)^{m+3} + \frac{2m+2}{2(4m+2)}\left(\frac{\kappa^2}{R}\right)^{2m+4} - (m+2)\left(\frac{\kappa^2}{R}\right)^2\right\} - \frac{\kappa^2}{R}\left\{\frac{1}{(2m+2)}\left\{\frac{m+5}{2m+6} + \frac{m+1}{2m+6}\left(\frac{\kappa^2}{R}\right)^{+3}\right\} + \frac{m-1}{(m+1)(m+3)}\left\{\frac{4m^4+32m^3+89m^2+97m+36}{16m^4+64m^3+76m^2+24m} + \frac{m+3}{4(m+2)}\left(\frac{\kappa^2}{R}\right)^{m+2} + \left(\frac{\kappa^2}{R}\right)^{2m+3}\left(\frac{1-4m+4m^2}{4(m+1)(2m+1)(2m+3)}\right) + \frac{2m^2+5m+3}{8m(2m+1)}\left(\frac{\kappa^2}{R}\right)^2\right\}\right\} - \frac{m-1}{2m}\left(\frac{\kappa^2}{R}\right)\left\{\frac{m}{2(m+1)(m+2)}\frac{m+4}{(2m+4)}\left(\frac{\kappa^2}{R}\right)^{m+2} + \frac{m+2}{2m+2}\left(\frac{\kappa^2}{R}\right)^{2m+2}\right\} + \frac{m^2+2m-2}{(m-1)(m+2)(m+3)}\left(\frac{\kappa^2}{R}\right)^{m+3}\left\{-\frac{m}{m(m+2)} + \frac{m-1}{2m+2}\left(\frac{\kappa^2}{R}\right)^{m+1} - \left(\frac{\kappa^2}{R}\right)^2\right\} + \frac{m^2+2m-2}{2(m+2)(m+3)(m-2)}\left(\frac{\kappa^2}{R}\right)^{m+4}\left\{-\frac{m-2}{2m} + \frac{m-2}{2m}\left(\frac{\kappa^2}{R}\right)^m - \left(\frac{\kappa^2}{R}\right)^2\right\}\right]. \quad (35)$$

expression of plug core radius R_{1p} for first order of α^2 is

$$R_{1p} = -\frac{\tau_1\big|_{r=R_{0p}}}{d(t)q(z)}, \quad (36)$$

with help of Eqs. (18), (29), (30) & (37), R_p can be written as

$$R_p = \kappa^2 + \alpha^2 m(q(z)d(t)R)^{m-1}R^2D\left[\frac{1}{(m+1)(m+3)}\left\{\left(\frac{m+3}{2}\right)\left(\frac{\kappa^2}{R}\right) - \left(\frac{\kappa^2}{R}\right)^{m+2}\right\} - \left(\frac{\kappa^2}{R}\right)\left(\frac{1}{m+2}\right)\left\{\left(\frac{m+2}{2}\right)\left(\frac{\kappa^2}{R}\right) - \left(\frac{\kappa^2}{R}\right)^{m+1}\right\} + \frac{m^2+2m-2}{(2m+4)(m+3)}\left(\frac{\kappa^2}{R}\right)^{m+3}\left(\frac{R}{\kappa^2}\right)^{m+2}\right]. \quad (37)$$

Formula for calculating pressure drop in arterial segment is

$$\Delta p = d(t)\int_0^L q(z)dz \quad (38)$$

Resistance to flow in artery is given by

$$\Lambda = \frac{d(t)\Delta p}{Q(t,z)} \quad (39)$$

Results

This section discusses effects of geometric & geological parameters such as ge, α, A & AC velocity, wall shear stress, core plug radius, pressure drop, strong gradient, and flow resistance. For analysis two values of index M have been selected. There was only 0.95 (for m<1) and a further 1.05 (for m>1) respectively. The ball Herschel-Ball of the bulkelley fluid [0.02, 0.04] is the width of the unbalanced fruit pressure parameter. (35) for solid state equation is subtracted

$$(m+2)R^{m+3}x^{m+3} - m(m+3)\theta R^{m+2}x^{m+2} - \frac{(m+2)(m+4)}{A}Q_s x^3 + (m^2+2m-2)\theta^{m+3} = 0. \quad (40)$$

Mathematically by using Newton-Raphson method, =values of q (z) = x are determined. Calculate the "X" values by taking Qs = 1 and 0.1 = 0.1,0.2. The stenotic field is z =0.5 and z = 1.5.

Illustration here. 2 (a) & (b) show the distribution of different core plug radios of =, m and A with m = 0.95, Q s = 1.0, and single = 0.2 single muscle fibers. Forms, and forms. In both cases it is observed that the plug core radius decreases when t is between 00-900 and 2700-3600. Conversely, it rises to 900–2700. And increasing the stress on yield increases the radius of the plug-core.

Figure 3 (a) & (b) show the axial variations of single and m = 0.95, t = 600, = 0.01 and Qs = 1.0 of the plug source. Honestly. In both cases the radius of the plug center shows activity that does not correspond to the stenosis frequency of the volume constant. The decrease along the given circular diameter is increased by A.

Photo 4. (A) & (b) show effect of different values on Qs = 1.0, m = 0.95, A = 0.2, = 0.01 and 0.1 = 0.1 radius smaller on axial plug distribution T. And type, respectively, the stenotic arteries. In both cases, plug main radius of t, [00, 3600] is showing a decreasing trend. Such reductions are known as single stenotic exercise.

The influence of various values of the tapping parameter axes on the spinal cord's axonal distribution in the muscle with Qs = 1.0, m = 0.95, 95 = 0.01, 0 = 0.1 and A =0.2 and = in the compartment itself. The fig is gone. 5. (A) respectively, and (b); The central radius plug hits smaller values of the weakened artery in both cases than the transverse and non-tapered arteries thereof. The inaccurate primary radio plug profile between the radio profile associated with it and the converter's plug core diaphragm is not affected.

Bar-The pressure on the rib of the wall decreases between 900 and 2700- 3600. Shear stress, however, follows a growing trend in shear stress where t [90 aller, 270.]. Photo 6. Designed to examine the effect of time by (a) and (b) on axial shear wall distribution;

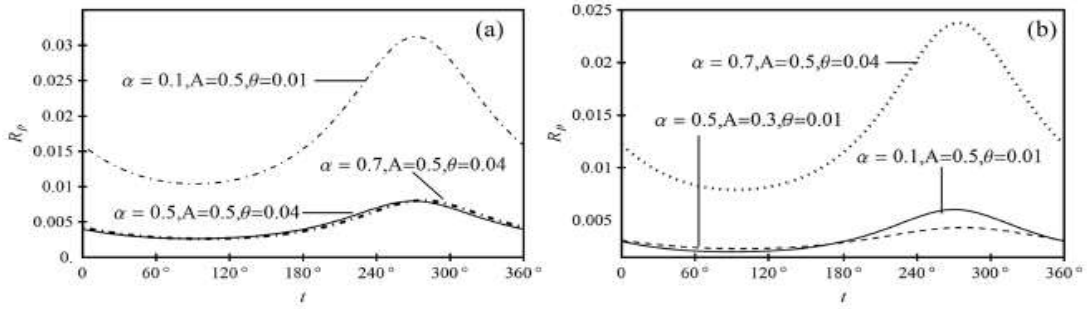

FIG. 2. Variation of plug core radius with time. (a) Single stenosis and (b) Overlapping stenosis.

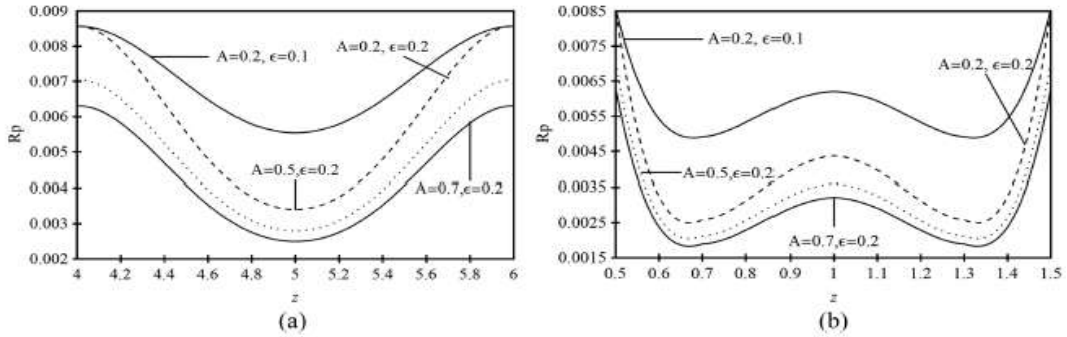

FIG. 3. Axial distribution of plug core radius. (a) Single stenosis and (b) Overlapping stenosis.

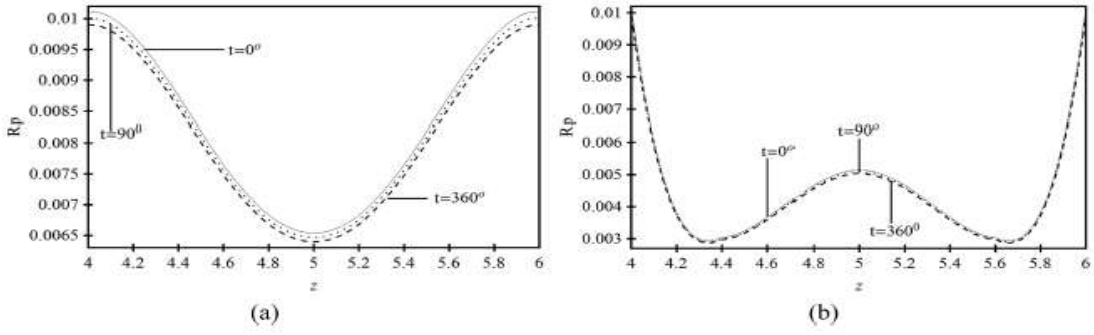

FIG. 4. Effect of time on the axial distribution of plug core radius. (a) Single stenosis and (b) Overlapping stenosis.

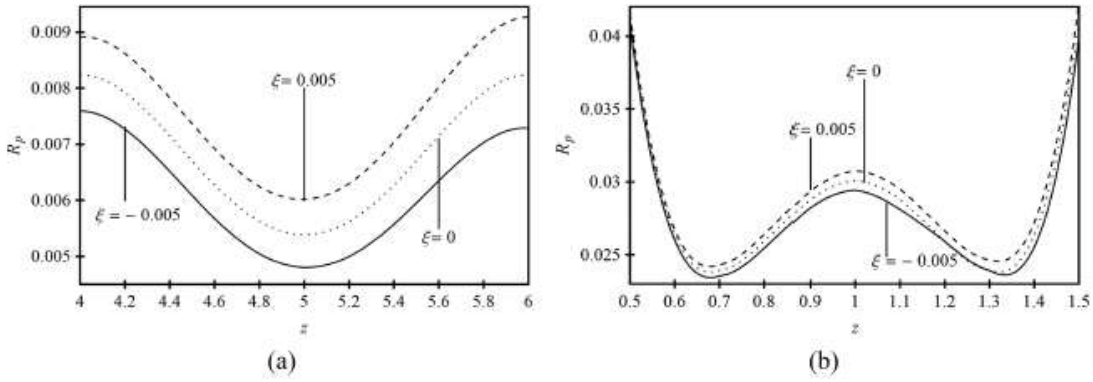

FIG. 5. Effect of tapering parameter ξ on the axial distribution of plug core radius. (a) Single stenosis and (b) Overlapping stenosis.

Qs = 1.0, m = 0.95, = 0,04, = 0,1, A = 0.5 and α = 0,2, respectively, for stenotic veins of small scale. Figs display the effects of A, α, and wall shear stress on the axial fluctuations. 1 And another one shaped in stone by arteries. 7. (A) and (b) respectively; other parameters are selected as m = 0.95, Qs = 1.0, 0 = 0.1, and t = 45. The yield stress parameter lies here as well as the pulsatile pressure gradient amplitude are assumed to improve the shear value. Pressing over the wall. By contrast, the shear stress decreases as it increases. Cues = 1.0, m = 0.95, = 0.1, 95 and A =. And 0,2 was developed for the thin, stent arteries. Here, the stress on wall shear is assumed to increase from the deviation to the shift in charge.

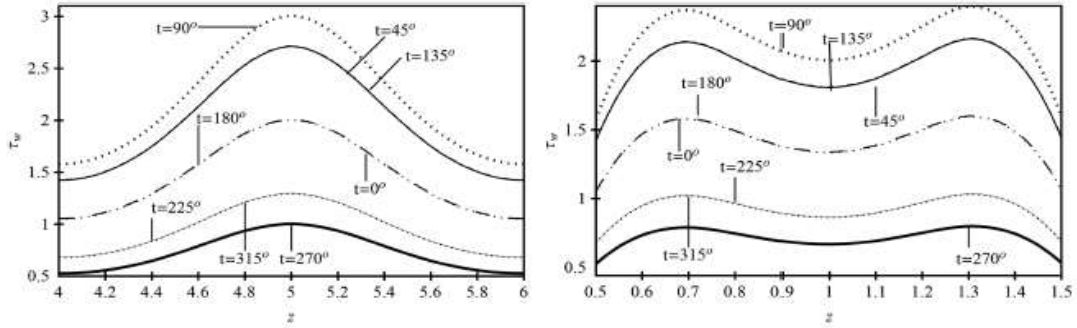

FIG. 6. Axial distribution of wall shear stress at different time instants. (a) Single stenosis and (b) Overlapping stenosis.

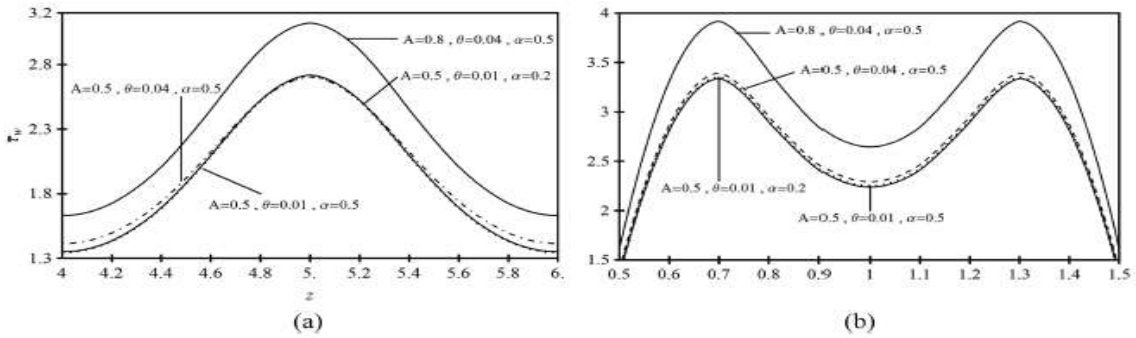

FIG. 7. Axial distribution of wall shear stress for different values of α, θ and A. (a) Single stenosis and (b) Overlapping stenosis.

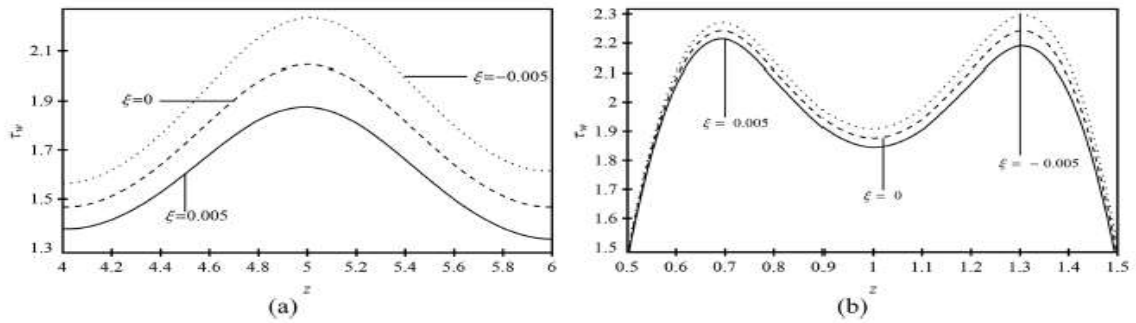

FIG. 8. Effect of tapering angle on wall shear stress. (a) Single stenosis and (b) Overlapping stenosis.

Picture 9 (A) and (b) indicate the time effect on the flow resistance axial plane for a person with Qs = 1.0, m = 0.95, = 0.01, = 0.1 and A = 0.2. Yeah, yeah. And the solid black, black pieces. In both cases the axial coordinate function z of the flow resistance can be seen to increase. Furthermore, when the core plugs radio and wall shear shear shear it follows the same procedure with the increase of T. By comparing the two figures it is also seen that the flow reaches the maximum values of a single stenotic artery.

Ed. Ed. 10. 10. (A) and (b) indicate a flow resistance time series with QS = 1.0, M = 0.95, 1 = 0.1, = 0.01 and A = 0.2. In both cases the values of increasing and enhancing flow resistance were found to increase.

Photo 11. (A) and (b) see the effect of the contact parameter, QS = 1.0 and =, 0.95, range = 0.01, range = 0.1 and range = 0.1 on the flow resistance axial transformation in the stenotic arteries. Both data indicate higher values for the arterial implant flow

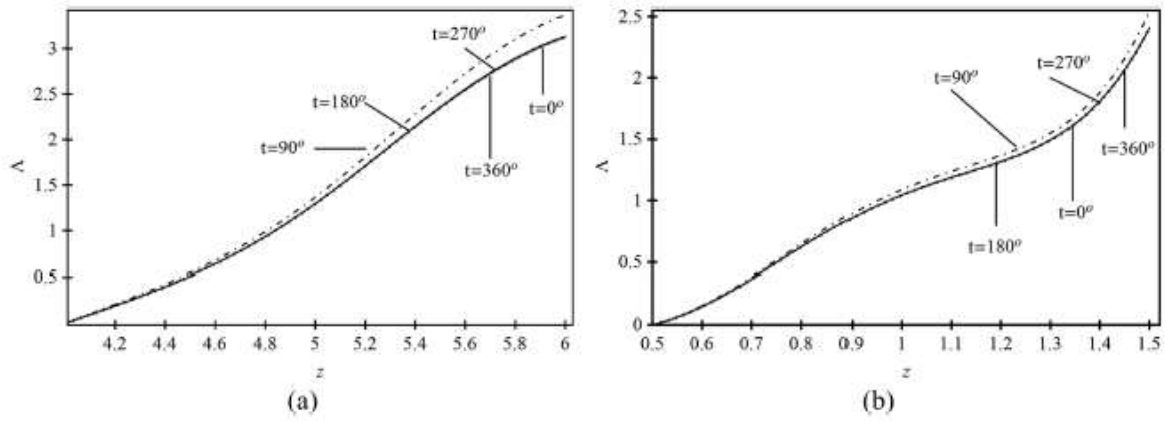

FIG. 9. Temporal effects on the resistance to the flow. (a) Single stenosis and (b) Overlapping stenosis.

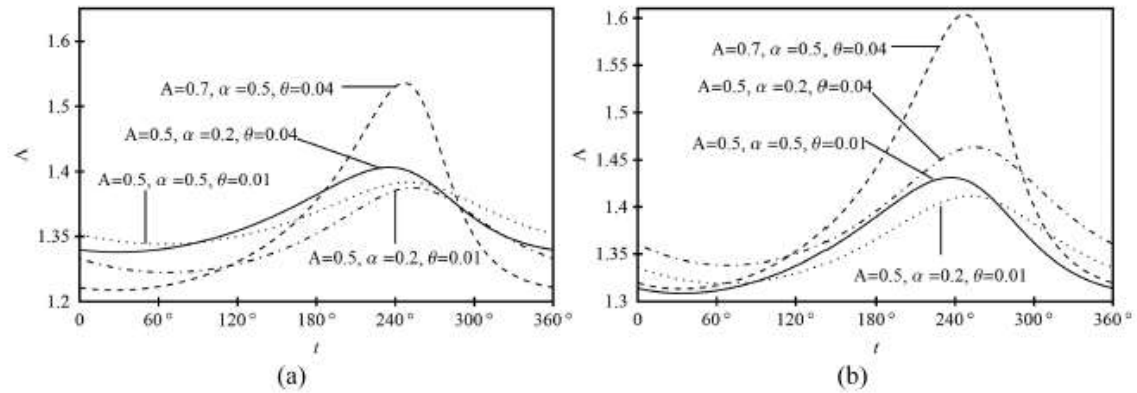

FIG. 10. Effects of A, α and θ on resistance to the flow. (a) Single stenosis and (b) Overlapping stenosis.

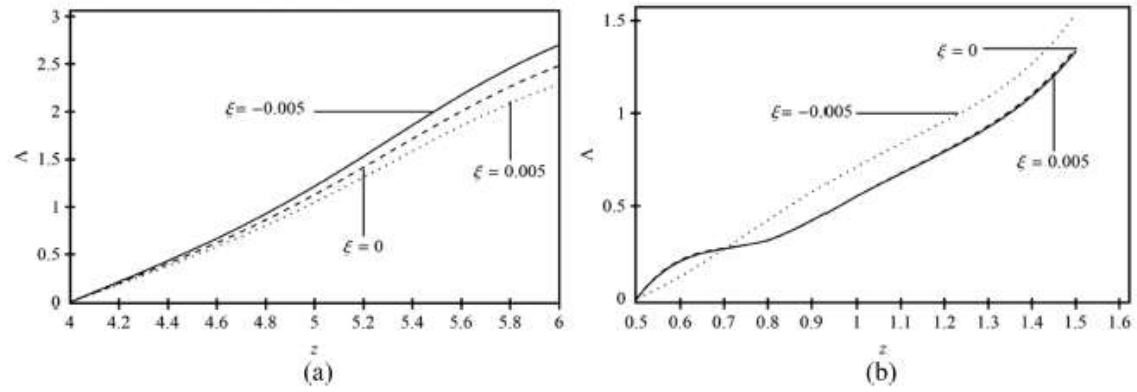

IG. 11. Effects of taper angle on axial distribution of resistance to the flow. (a) Single stenosis and (b) Overlapping stenosis.

Instead of distal arteries and arteries which are not sealed. Indeed replacing an enlarged artery is minimal. Also, it was found that the metal flow resistance is lower than that of the single iron artery. The results of single-stenosis arterial compression are shown in panel (a), whereas panel (b) shows the result of passage of the hair artery.

Illustration. 12 Displays the effects of the axial fluctuations of m = 0.95, Qs = 1.0, = 0.1, A = 0.2 0.01 =

0.01. The pressure gradient in both cases is at least strong enough to bend the artery, and the maximum to bend the artery. Comparison of the two panels shows that, in bending the hair artery, Q (z) reaches greater values.

Photo 13. QS = 1.0, M = 0.95, = 0.1, 0.01 = 0.01 and A = 0, 2. The stenotic arteries are both single and large. The arp is too small to bend the artery, and too big to bend the artery, close to Q (z).

Deviation and Convergence Profiles for the exercise include the vein profile deviation.

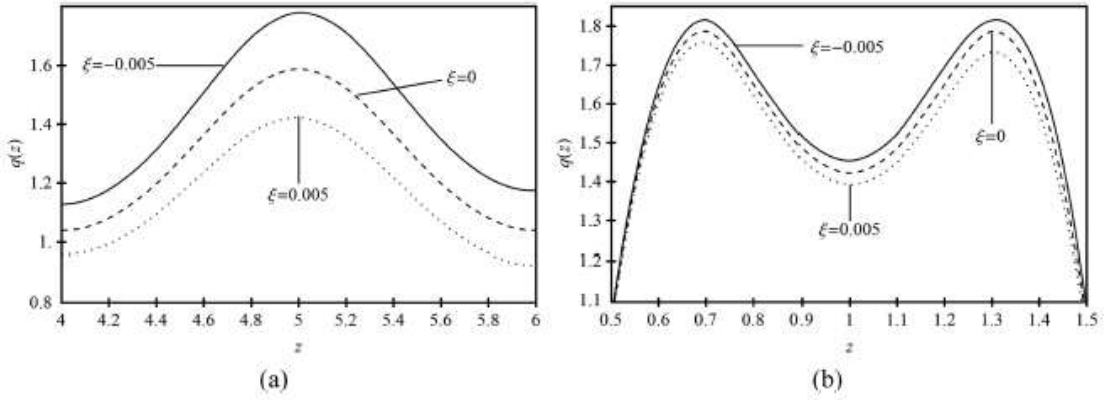

FIG. 12. Axial variation of $q(z)$ for different values of taper angle. (a) Single stenosis and (b) Overlapping stenosis.

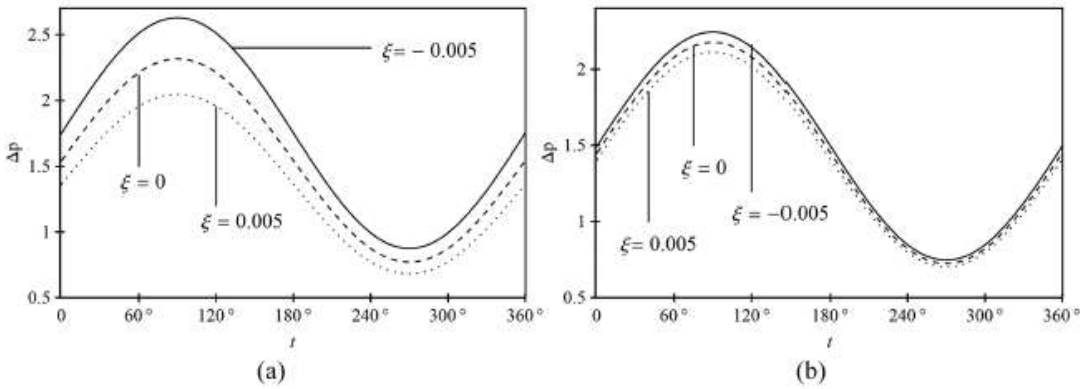

FIG. 13. Temporal distribution of pressure drop for different values of taper angle. (a) Single stenosis and (b) Overlapping stenosis.

Conclusion

In a vascular-shaped stenotic-shaped area, the unstable pulsatile flow of extracellular blood is analysed. Herschel-The bulkley type fluid is used in small blood vessels to assess the non-Newtonian blood fraction. The standard deviation method can be used to solve nonlinear governing equations of the current flow problem. The present study may reveal stress on yield, stenosis and blood vessel structure in the blood. The main findings of the research under consideration are given below :

- The increase in the core radius of the rod plug may be attributed to the increasing values of the infinite yield pressure. A decrease in the plug core 's radiation potential can be detected through increasing the stenosis severity. It is also worthy of note that the core radius of the plug is a reduced time feature. Radius core plug. Compared with anterior plexus and non-tapped arteries, this damaged artery achieves smaller flexibility values.
- Period stress is a constant function of the time of shear stress [0-, 90- and [270-360]. This, however, is a relaxation time reduction function [90, 270]. Prices increase the stress on yields Boost shear stress on the wall. By turning the artery in the duct into a wall. The shear stress in bending the tapped artery is big but small. The stress of yield and the parameter of the shear frequency lead to resistance in flow. The effect of T on the flow resistance is similar to that of T on the shear stress on the wall. Additionally, as the flow increases, the resistance decreases, from 0.005 to 00.005. It can be observed that the resistance to the N-shaped stenosis is greater for converting the damaged artery to z = 0.7 than for replacing the damaged artery with its counterparts. Z = 0.7 Differences in flow and higher resistance values are obtained after resistance for the tapered arteries, while the reverse trend appears to change for the tapered arteries. For the conversion of the enlarged artery and dilated artery the pressure drop and the continuous pressure gradient are greater.
- The pressure of yield increases and the frequency parameter worsens causes the flow to be limited. The effect of increasing the T on flow resistance is similar to that of the T shear stress on the wall. As the flow drops from 0.005 to 00.005, so does the flow resistance. Even with the stenosis scale , high vascular artery variance is the flow resistance and the reverse tapered artery is as high as z = 0.7 compared with its counterparts. The flow resistance in the rotating arteries after Z = 0,7 achieves

lower deviation and lower values, but tectonic patterns can be observed by adjusting the exercise applied.

- The reduction of pressure is minimal by changing the visual pressure of the body and deforming the damaged artery, and is ideal to replace damaged arteries.

References

1. Dwivedi, P., Pal, T.S. and Rakesh, L. (1982). Micropolar fluid model for blood flow through a small tapered tube, Indian J. Technology 20: 295–299.
2. Chaturani, P. and Pralhad, R.N. (1985). Blood flow in tapered tubes with biorheological applications, Biorheology 22(4): 303–314.
3. Tu, Deville *et al*. (1992). Finite element simulation of pulsatile flow through arterial stenosis, J. Biomechanics 25(10): 1141–1152.
4. Lee, J. and Fung, Y. (1970). Flow in locally constricted tube at low Reynolds number, J. Appl. Mech., 379–16.
5. Azuma, T. and Fukushima, T. (1976). Flow patterns in stenotic blood vessel models, Biorheology. 13: 337–355.
6. Morgan, E. and Young, D.F. (1974). An integral method for the analysis of flow in Arterial stenosis, Bull Math. Biol. 36: 39–53.
7. Cheng, L.C., Robertson, J.M. and Clark, M.E. (1973). Numerical calculations of plane oscillatory non-uniform flow—II. Parametric study of pressure gradient and frequency with square wall obstacles, J. Biomechanics 6: 521–538.
8. Padmanabhan, N. (1980). Mathematical model of arterial stenosis, Med. Biol. Engng Comput. 18: 281–286.
9. Kawaguti, M. and Hamano, A. (1983). Numerical study on post-stenotic dilatation, Biorheology 20: 507–518.
10. O'Brien, V. and Ehrlich, L.W. (1985). Simple pulsatile flow in an artery with a constriction, J. Biomechanics, 18: 117–127.
11. Nadeem, S., Akbar, N.S., Hendi, A.A. and Hayat, T. (2011). Power law fluid model for blood flow through a tapered artery with a stenosis, Appl. Math. Comput. 217: 7108–7116.
12. Chaturani, P. and Ponnalagar Samy, R. (1986). Pulsatile flow of a Casson fluid through stenosed arteries with application to blood flow, Biorheology, 23: 499–511.
13. Mirza, A., Abdul Hameed, M. and Shafie, S. (2017). Magnetohydrodynamic approach of non-Newtonian blood flow with magnetic particles in stenosed artery, Applied Mathematics and Mechanics (English Edition), 38: 379–392.
14. Shukla, J.B., Parihar, R.S. and Rao, B.R.P. (1980). Effects of stenosis on non-Newtonian flow through an artery with mild stenosis, Bull. Math. Biol., 42: 283–294.
15. Zaman, A. and Ali, N. (2016). Effects of peripheral layer thickness on pulsatile flow of Herschel–Bulkley fluid through a stenotic artery, Can. J. Phys., 94(9): 920-928.
16. Zaman, A., Ali, N., Anwar Beg, O. and Sajid, M. (2016). Heat and mass transfer to blood flow through a tapered overlapping stenosed artery, International Journal of Heat and Mass Transfer, 95: 1084–1095.
17. Zaman, A., Ali, N., Sajid, M. and Hayat, T. (2015). Effects of unsteadiness and non-Newtonian rheology on blood flow through a tapered time-variant stenotic artery, AIP Advances, 5: 037129.
18. Ali, N., Zaman, A. and Sajid, M. (2014). Unsteady blood flow through a tapered stenotic artery using Sisko model, Computers & Fluids, 101: 42–49.
19. Ali, N., Zaman, A., Sajid, M., Nieto, J.J. and Torres, A. (2015). Unsteady non-Newtonian blood flow through a tapered overlapping stenosed catheterized vessel, Mathematical Biosciences 269: 94–103.
20. Zaman, A., Ali, N., Anwar Beg, O. and Sajid, M. (2016). Unsteady two-layered blood flow through aw-shaped stenosed artery using the generalized Oldroyd-B fluid model, ANZIAM Journal, 58: 96–118.
21. Zaman, A., Ali, N. and Sajid, M. (2016). Slip effects on unsteady non-Newtonian blood flow through an inclined catheterized overlapping stenotic artery, AIP Advances, 6: 015118.
22. Shah, S.R. (2013). An innovative study for non-Newtonian behaviour of blood flow in stenosed artery using Herschel-Bulkley fluid model, International Journal of Bio-Science and Bio-Technology, 5: 233–240.
23. Nikolov, S., Stoytchev, S., Torre, A. and Nieto, J.J. (2003). Biomathematical modeling and analysis of blood flow in an intracranial aneurysm, Neurological Research, 25: 497–504.
24. Sankar, S. and Lee, U. (2009). Mathematical modeling of pulsatile flow of non-Newtonian fluid in stenosed arteries, Commun Nonlinear Sci Numer Simul, 14:2971–2981.
25. Siddiqui, S.U., Verma, N.K., Mishra, S. and Gupta, R.S. (2009). Mathematical modelling of pulsatile flow of Casson's fluid in arterial stenosis, App Math Comp., 210: 1–10.
26. Chakravarthy, S. and Mandal, P.K. (1994). Mathematical modelling of blood flow through an overlapping stenosis, Math. Comput. Model., 19: 59–73.
27. Srivastava, V.P. and Rastigi, R. (2010). Blood flow through stenosed catheterized artery: Effects of hematocrit and stenosis shape, Comput. Math. Applc., 59: 1377–1785.
28. Maruthi, K.P., Vijaya, B. and Umadevi, C. (2014). A mathematical model of Herschel-Bulkley fluid through an overlapping stenosis, IOSR Journal of Mathematics (IOSR-JM), 10(2): 41–46.
29. Srikanth, J.V., Ramana Reddy, S. Jain, and Kale, A. (2015). Unsteady polar fluid model of blood flow through tapered-shape stenosed artery: Effects of catheter and velocity slip, Ain Shams Engineering Journal, 6: 1093–1104.
30. 30. Sankar, D.S. and Hemalatha, K. (2006). Pulsatile flow of Herschel–Bulkley fluid through stenosed Arteries–A mathematical model, International Journal of Non-Linear Mechanics, 41: 979–990.